Titanium Carboxylate Molecular Layer Deposited Hybrid Films as Protective Coatings for Lithium-ion Batteries

Sofie S. T. Vandenbroucke,[†,‡] Lowie Henderick,[†] Louis L. De Taeye,[‡,¶] Jin Li,[†] Karolien Jans,[‡] Philippe M. Vereecken,[¶,‡] Jolien Dendooven,[†] and Christophe Detavernier*[,†]

†*Department of Solid State Sciences, Ghent University, Krijgslaan 281 (S1), 9000 Gent, Belgium*

‡*imec, Kapeldreef 75, B-3001 Leuven, Belgium*

¶*Centre for Surface Chemistry and Catalysis, KU Leuven, Celestijnenlaan 200F, B-3001 Leuven, Belgium*

E-mail: christophe.detavernier@ugent.be

Abstract

The lifetime of lithium-ion batteries can be extended by applying protective coatings to the cathode's surface. Many studies explore atomic layer deposition (ALD) for this purpose. However, the complementary molecular layer deposition (MLD) technique might offer the benefit of depositing hybrid coatings that are flexible and can accommodate potential volume changes of the electrode during charging and discharging of the battery. This study reports the deposition of titanium carboxylate thin films via MLD. The structure and stability of the hybrid films is studied using Fourier Transform IR spectroscopy. The electrochemical properties of two titanium carboxylate films and

Vandenbroucke, Sofie ST, Lowie Henderick, Louis L. De Taeye, Jin Li, Karolien Jans, Philippe M. Vereecken, Jolien Dendooven, and Christophe Detavernier. "Titanium Carboxylate Molecular Layer Deposited Hybrid Films as Protective Coatings for Lithium-Ion Batteries." ACS Applied Materials & Interfaces (2022).
Full text (Publisher's DOI): *https://doi.org/10.1039/D0NR02444A*

a 'titanicone' MLD film, deposited using TDMAT and glycerol, are evaluated on top of a TiO_2, TiN and $LiMn_2O_4$ electrode. The coatings are found to present good lithium-ion kinetics and to reduce electrolyte decomposition. Overall, the titanium carboxylate films deposited in this work seem promising as protective and elastic coatings for future high-energy lithium-ion battery cathodes.

Keywords

MLD, lithium-ion battery, surface modification, hybrid, titanium

1 Introduction

The world as we know it today, full of mobile and wireless technology, would not exist without the invention of the lithium-ion battery. Now, 30 years after the release of the first commercial lithium-ion battery, their complex ageing process leading to capacity fading is still one of the major concerns in battery research.[1–4] The main phenomena causing ageing of the cathode material are transition metal dissolution, electrolyte decomposition and volume changes of the active material upon (dis)charging.[4–6] To suppress these effects, a protective coating can be applied to the cathode surface to eliminate direct contact with the electrolyte solution.[7–9]

For this purpose, atomic layer deposition (ALD) is of great interest. The vapor-phase deposition technique based on alternating self-limiting surface reactions, produces pinhole free and conformal thin films on complex 3D-substrates such as a powder-based lithium-ion battery cathode.[10–12] The most extensively studied coating is ALD Al_2O_3 which effectively increases the battery lifetime, but hinders the kinetics due to its poor lithium-ion conductivity.[13–16] In addition, the inorganic materials deposited by ALD are rigid and may crack upon volume expansion of the cathode.[17]

More flexible films can be deposited with the organic alternative of ALD, called molecular layer deposition (MLD). The technique relies on the same principle as ALD and is used to deposit organic or hybrid inorganic/organic thin films with molecular precision.[18–21] One group of hybrid MLD materials are the so called 'metalcones', created by the combination of a metal containing precursor and an alcohol.[22] Also hybrid metal carboxylate films can be grown with MLD, by using carboxylic acids as organic precursor. For instance, Klepper et al.[23] deposited aluminium carboxylate films using trimethylaluminium (TMA) and seven different saturated dicarboxylic acids: oxalic, malonic, succinic, glutaric, pimelic, suberic and sebacic acid. A titanium carboxylate film was grown by Momtazi et al.[24] using tetra-isopropoxide (TTIP) and succinic acid.

To our knowledge apart from metalcones, MLD films remain to be explored as protective and flexible coatings for lithium-ion batteries. The reader is referred to the review papers of Zhao et al.[25,26] and Ban et al.[17] to obtain an overview of the current status of MLD for lithium-ion batteries. Thin alucone films were found to stabilize the electrode surface of Si nanoparticles, sulfur and metallic lithium, and were able to accommodate the volume expansion of the electrode without breakage.[27–32] Also zincone MLD films are reported to improve the cycling stability of high capacity Si electrodes, presenting a volume change of approximately 400 % during cycling.[33] In addition, Piper et al.[28] reported that the use of aromatic organic precursors for MLD such as hydroquinone (HQ) leads to an improved mechanical strength and conductivity of the protective coating on top of Si anodes.

In this work, MLD titanium carboxylate thin films are deposited using tetrakis(dimethylamino)titanium(IV) (TDMAT) and various dicarboxylic acid precursors: oxalic acid, malonic acid, succinic acid, glutaric acid and 3,6-dioxaoctanedioic acid. The latter contains two ethylene oxide units per molecule, which could potentially increase the lithium-ion conductivity.[34] First, the growth of the films is studied using in situ ellipsometry. Next, the structure and stability of the films is investigated, and a comparative

study is made of the electrochemical properties of two MLD titanium carboxylate and a titanicone thin film on top of a TiO_2, TiN and $LiMnO_2$ electrode.

2 Experimental

MLD depositions are performed inside a home-built vacuum reactor with a base-pressure of 1×10^{-6} mbar. The samples are mounted onto a PID-controlled copper heating stage and heated up to 100 °C, unless mentioned otherwise. Tetrakis(dimethylamino)-titanium(IV) (TDMAT, $Ti(NMe_2)_4$, 99 % Strem Chemicals Inc.) is used as titanium precursor at a temperature of 45 °C. Various dicarboxylic acids are used as organic precursor to grow titanium carboxylate films: oxalic acid ($\geq$ 99 %, Sigma Aldrich), malonic acid (99 %, Sigma Aldrich), succinic acid ($\geq$ 99 %, Sigma Aldrich), glutaric acid (99 %, Sigma Aldrich) and 3,6-dioxaoctanedioic acid (2,2'-[ethylenebis(oxy)] bisacetic acid, Sigma Aldrich) and heated inside a glass container to 100 °C, 80 °C, 100 °C, 90 °C and 30 °C respectively. A schematic drawing of all precursors can be found in Figure 1 a. Titanicone MLD films are grown using glycerol (GL, $\geq$ 99.5 %, Sigma Aldrich) as organic precursor, heated in a stainless steel container to 65 °C.[35] Argon ($\geq$ 99.9999 %, Air Liquide S.A.) is used as carrier gas to pulse the vapour of the organic precursors into the reactor chamber at a pressure of 5×10^{-3} mbar. A standard pulse time of 60 s is used for both precursors in the MLD process, followed by a pump time of 90 s for the TDMAT and 100 s for the organic precursor to evacuate the chamber back to its base pressure. The titanicone process is observed to grow at a rate of 0.07 nm/cycle.

In situ spectroscopic ellipsometry is performed with a J.A. Woollam M-2000 ellipsometer to monitor the film thickness during MLD. The thickness is fitted using a Cauchy model in the CompleteEASE software (J.A. Woollam Co.) and validated by X-ray reflectivity (XRR) measurements performed using a Bruker D8 diffractometer with a Cu K-alpha X-ray source and a point detector. In situ ellipsometery is used to determine the saturation behaviour of

the MLD half cyles on top of a Si substrate. The exposure time for each precursor is varied separately and at least 20 MLD cycles are grown with each set of parameters. The growth per cycle (GPC) is determined by a linear fit to the final 10 cycles of the growth curve.

Fourier transform IR measurements (FTIR) are performed on Si coated substrates using a Vertex 70V spectrometer (Bruker Co.) with a DLaTGS detector. The spectrometer is pumped to vacuum (approximately 1×10^{-2} mbar) for at least 15 min in order to obtain a constant background level of atmospheric gases inside the sample compartment. The IR-signal is detected for a measurement time of 5 min with a resolution of $4\,\mathrm{cm}^{-1}$. A measurement of a blank Si reference is subtracted from the raw data.

X-ray photoelectron spectroscopy (XPS) measurements are performed with a Theta Probe XPS instrument (Thermo Fischer Scientific Inc.) using a monochromatic Al K-alpha X-ray source in an ultra high vacuum chamber with a base pressure of 2×10^{-10} mbar. The spectra are analysed using the CasaXPS software package. The C−C/C−H component is not used for calibration due to the complexity of the carbon spectrum, resulting from a combination of the organic ligands inside the MLD films and adventitious carbon. Instead the spectra are calibrated by setting the O−Ti component in the O1s spectrum at 530.0 eV.[36] The error on the atomic concentrations is estimated to be roughly 10 % of the reported value.

Electrochemical characterization is carried out inside an argon filled glovebox (H_2O < 1 ppm, O_2 < 1 ppm) using a three electrode setup and a home-built potentiostat/galvanostat.[37] A solution of 1 M $LiClO_4$ in propylene carbonate (99.7 %, Sigma Aldrich) is used as electrolyte. Li-strips (99.9 %, Sigma Aldrich) are used as counter and reference electrodes. Thin MLD films are deposited on top of a TiO_2, TiN and $LiMn_2O_4$ electrode stack, to be used as working electrodes. The TiO_2 electrode stack consists of Si, 20 nm SiO_2, 40 nm PVD TiN and 40 nm anatase TiO_2. The TiN electrode constitutes a stack of Si, 20 nm SiO_2 and 150 nm PVD TiN. And the $LiMn_2O_4$ electrode stack consists of Si, 60 nm PVD

TiN, 80 nm PVD Pt and 100 nm PVD $LiMn_2O_4$, deposited as described by Put et al.[38] A total surface area of 1.05 cm^2 of the working electrode with the thin MLD film on top is exposed to the liquid electrolyte.

3 Results and Discussion

Titanium carboxylate deposition. In situ ellipsometry experiments are carried out to analyse the thin film growth of each process at a substrate temperature of 100 °C. The results in Figure 1 display good saturation behaviour for the TDMAT-oxalic acid process (Figure 1 b) with a GPC of 0.27 nm/cycle. For the TDMAT-malonic acid process also good saturation behaviour seems to be achieved (Figure 1 c), but the GPC is found to vary as a function of the ageing of the malonic acid. In addition, the malonic acid precursor changes from a white powder into a yellow liquid during process operation. Both observations indicate that the malonic acid is not stable at the used temperature and pressure. Most likely the malonic acid is decarboxylated and acetic acid is formed as a by-product.[39–41] Unfortunately, the by-product acetic acid is not compatible with the o-rings used inside the pumping system of the MLD reactor and the malonic acid process is thus not further investigated.

For the other MLD processes using succinic acid, glutaric acid and 3,6-dioxaoctanedioic acid, good saturation behaviour is observed for the dicarboxylic acid precursor pulse while the TDMAT pulse includes a parasitic CVD component (Figure 1 d-f). Using a standard pulse time of 60 s an average GPC of 0.09 nm/cycle, 0.07 nm/cycle and 0.06 nm/cycle is obtained respectively. Acid by-products might be formed during the process, which may affect the GPC. However, the impact of etching side reactions is considered to be small as the saturation experiments show that the films are not completely etched upon prolonged exposure times.

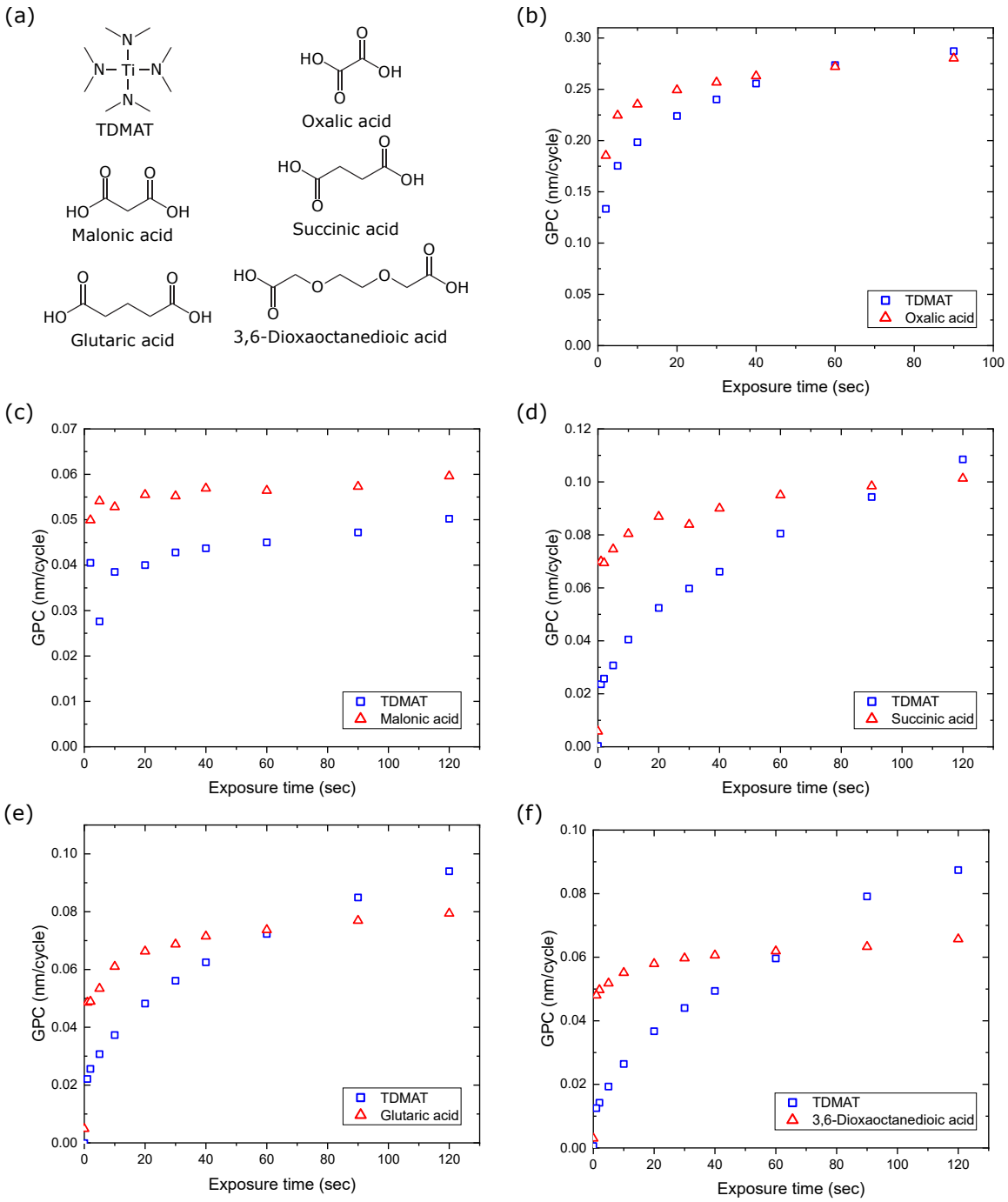

Figure 1: All precursors used in this work (a) and the growth per cycle (GPC) of the TDMAT/oxalic acid (b), TDMAT/malonic acid (c), TDMAT/succinic acid (d), TDMAT/glutaric acid (d) and TDMAT/3,6−dioxaoctanedioic acid (f) process at a sample temperature of 100 °C as a function of precursor exposure time. The GPC is monitored using in situ ellipsometry.

The saturation behaviour of all TDMAT/dicarboxylic acid processes is also investigated at 160 °C (data in Figure S1 in the supporting information). Again good saturation behaviour is observed only for the TDMAT/oxalic acid process, while a parasitic CVD component is present during the TDMAT-pulse for the other dicarboxylic acid processes. The GPC of all processes, using a standard pulse time of 60 s, drops with increasing temperature to 0.16 nm/cycle, 0.08 nm/cycle, 0.06 nm/cycle and 0.05 nm/cycle for the TDMAT/oxalic acid, TDMAT/succinic acid, TDMAT/glutaric acid and TDMAT/3,6-dioxaoctanedioic acid process respectively. In literature, this decrease in GPC with increasing temperature is typically attributed to a reduction of the number of active reaction sites, higher desorption rate of the organic precursor molecules and less infiltration of the precursors into the film.[20,42–45] An increase in refractive index of 6 % to 11 % and increase in density of 14 % to 23 % with increasing temperature is observed for all processes (Table S1 in supporting information). X-ray photoelectron spectroscopy (XPS) measurements of the TDMAT/oxalic acid films grown at 100 °C and 160 °C (Figure S2 in supporting information) show that this trend is associated with a decrease in carbon content and an increase in titanium concentration. A possible explanation could be a change in coordination mode of both precursors e.g. higher amount of double reactions at higher temperature as was observed by Yoon et al.[44] for the deposition process with diethylzinc (DEZ) and ethylene gycol (EG), leading to a lower organic content and higher density.

Structure. The chemical bonds present in the thin films are investigated using FTIR. The as-deposited thin films in Figure 2 all present similar features. A broad band can be observed at 3600 cm^{-1} to 2500 cm^{-1} from the O−H stretching vibration as a result of hydrogen bonded OH-groups.[46,47] These OH-groups might originate from unreacted dixarbocylic acid molecules, dimers or absorbed water molecules from exposure to ambient atmosphere. Superimposed on this broad band, several peaks are visible at 2950 cm^{-1}, 2865 cm^{-1}, 2930 cm^{-1} and 2855 cm^{-1} which can be assigned to the asymmetric and symmetric CH_3 and CH_2 stretching vibration respectively.[46,48] Inevitably these are partially the result of organic contamination

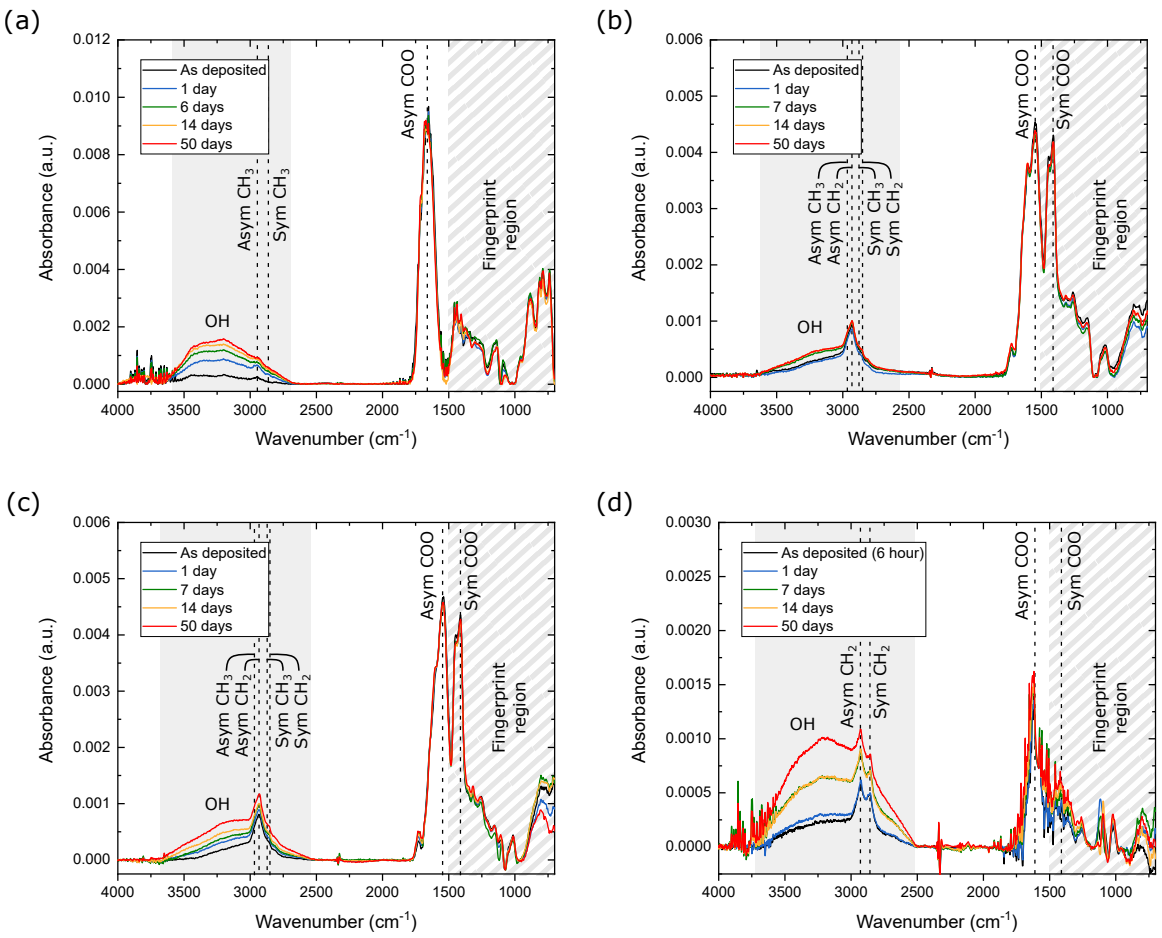

Figure 2: FTIR spectra of the thin TDMAT/oxalic acid (a), TDMAT/succinic acid (b), TDMAT/glutaric acid (c) and TDMAT/3,6−dioxaoctanedioic acid (d) films as deposited and for different time intervals up to 50 days of air exposure under ambient laboratory conditions.

from air exposure, but the high intensity of the CH_2 stretching vibration for the succinic acid, glutaric acid and 3,6-dioxaoctanedioic acid films confirms the presence of an alkane chain being built into the film. The most prominent features in the FTIR spectra can be found between 1650 cm^{-1} to 1400 cm^{-1}, originating from the asymmetric and symmetric vibration of the carboxylate anion.[48–53] The exact peak position for the different films can be found in Table 1. For the oxalic acid film only one dominant peak is observed at 1653 cm^{-1}. The frequency is too low to be ascribed to the C=O stretching vibration and the peak is more likely identified as the asymmetric COO stretching vibration.[47,48,54,55] The symmetrical

stretching vibration might be assigned to one of the features appearing between 1460 cm^{-1} to 1400 cm^{-1}, but as described later peak identification in this region is rather complex mainly due to overlap with the CH bending modes.[51,54] All features are consistent with the successful incorporation of the organic dicarboxylic acid molecules into the film.

Table 1: The peak position of the asymmetric (as.) and symmetric (sym.) carboxylate stretching vibration (COO) and their splitting Δ observed in the FTIR spectra of the as-deposited films (cm^{-1}).

	TDMAT/ oxalic acid	**TDMAT/ succinic acid**	**TDMAT/ glutaric acid**	**TDMAT/ 3,6−dioxaoctanedioic acid**
Asym COO	1653	1547	1539	1617
Sym COO	1460 to 1400	1409	1411	1408
Splitting Δ	193 to 253	138	128	209

The width of the frequency splitting Δ between the asymmetric and symmetric carboxylate stretching vibration, can provide information about the coordination of the carboxylate ions to the metallic Ti centre. For chelating complexes Δ is between 50 cm^{-1} to 150 cm^{-1}, bridging complexes have a Δ between 130 cm^{-1} to 200 cm^{-1} and a large $\Delta > 200\,cm^{-1}$ is observed for unidentate complexes.[56–58] The values for Δ in Table 1 indicate a combination of chelating and bridging complexes for the succinic and glutaric acid thin films. In contrast, the reaction between TDMAT and oxalic acid or 3,6-dioxaoctanedioic acid would be of unidentate type.

Peak identification in the so-called 'fingerprint region' below 1500 cm^{-1}, is cumbersome as many molecules posses bands in this region which frequently overlap. Two bands from the C−O−C stretching vibration of the ethylene oxide units in the 3,6-dioxaoctanedioic acid molecule are expected in the range from 1150 cm^{-1} to 1060 cm^{-1} and 1040 cm^{-1} to 900 cm^{-1}.[46,59] It is difficult to identify these features in the fingerprint region with utmost certainty and FTIR can thus not be used to conclude the successful incorporation of the ethylene oxide units into the TDMAT/3,6-dioxaoctanedioic acid thin film. However, in anticipation of the XPS results in the next paragraph, the XPS data indicate the presence of

a larger concentration of C−O bonds compared to the other titanium carboxylate films.

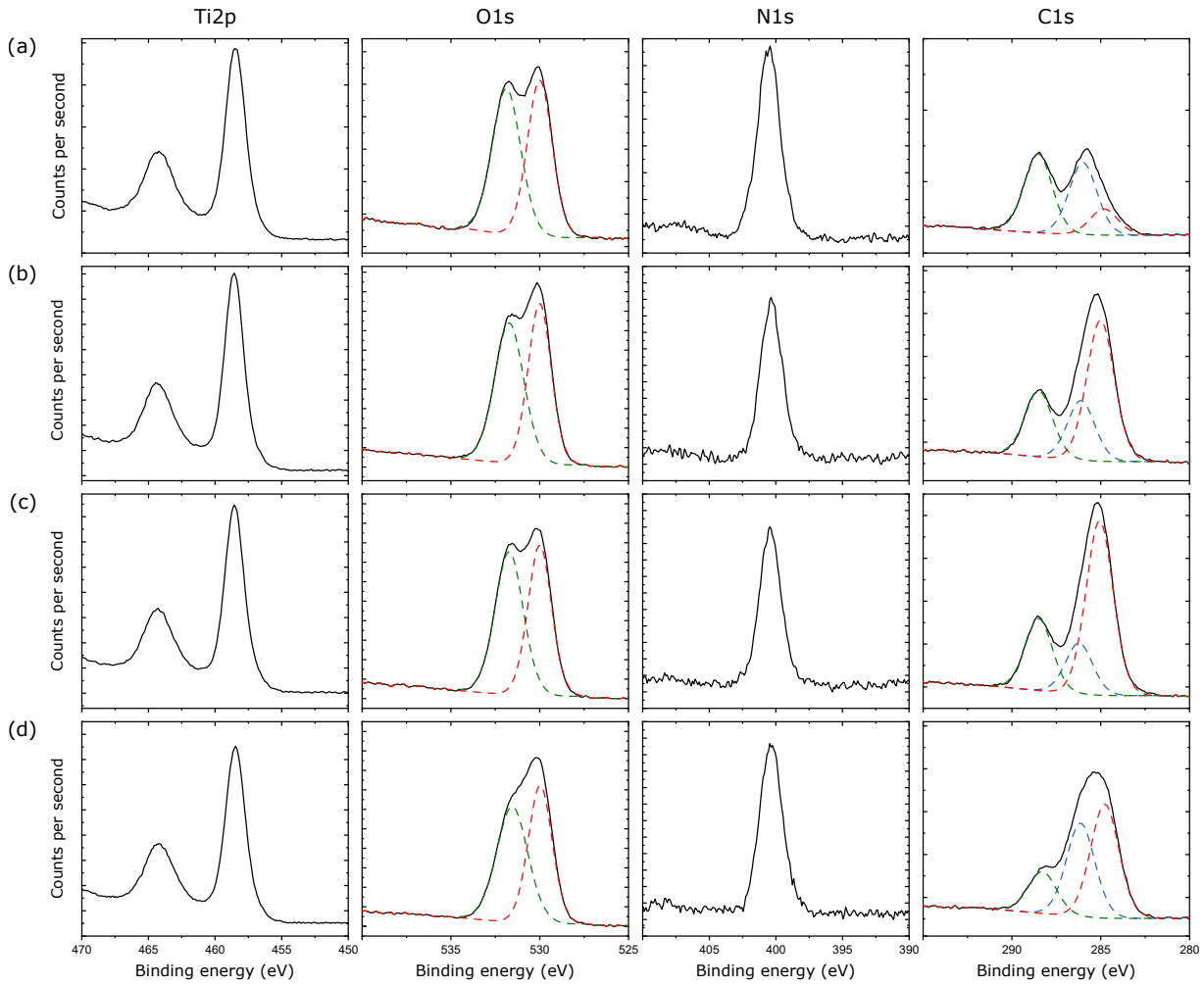

Figure 3: XPS spectra of the thin TDMAT/oxalic acid (a), TDMAT/succinic acid (b), TDMAT/glutaric acid (c) and TDMAT/3,6−dioxaoctanedioic acid (d) films. The O1s spectrum is split into two components: O−Ti (red, 530.0 eV) and OOC (green, 531.5 eV to 531.9 eV). The C1s spectrum is split into three components: COO (green, 288.3 eV to 288.5 eV), C−N/C−O (blue, 286.0 eV to 286.2 eV) and C−C/C−H (red, 284.8 eV to 285.0 eV).

Composition of the films by XPS. XPS measurements are performed on all titanium carboxylate films deposited at 100 °C. The data are shown in Figure 3 and Table 2 is used to discuss the composition of the films. It has to be noted that determination of the exact stoichiometry via XPS is difficult due to the large measurement error of roughly 10 % on the atomic concentrations and the exposure of the samples to air which will influence the C and

O content. Argon sputtering of these films to remove the top surface is not possible due to preferential sputtering of the lighter elements in the Ti-based film.[60,61]

The Ti2p spectra show the $Ti2p_{2/3}$ peak at 485.5 eV to 458.6 eV and the $Ti2p_{1/2}$ peak at 464.2 eV to 464.3 eV, suggesting the presence of Ti(IV) oxide.[36] The O1s spectra can be split into two components with a low energy component at 530.0 eV, being the O−Ti component used for calibration of the spectra. The second component at a higher binding energy of 531.5 eV to 531.9 eV can be assigned to OOC of the carboxylate ion.[62–65] In the N1s spectra a peak is visible at 400.3 eV to 400.5 eV which can be assigned to N−C groups of the protonated ligands of TDMAT adhered to the surface. This is also observed during the thermal ALD process using TDMAT and water.[66,67]

The C1s spectra can be fitted using three components. The low energy component at 248.8 eV to 285.0 eV is assigned to the presence of C−C and C−H. Inevitably this peak is partially arising from adventitious carbon, present due to air exposure. However, a clear increase can be observed with increasing carbon chain length of the used carboxylic acid precursor. The second component at 286.0 eV to 286.2 eV is identified as C−O and C−N bonds originating from the presence of the carboxylate ion and contamination of the TDMAT ligands respectively.[62,63,66,68] The atomic percentage of this peak is higher for the TDMAT/3,6−dioxaoctanedioic acid film, indicating the presence of intact ethylene oxide units inside the deposited film. The high energy component at 288.3 eV to 288.5 eV in the C1s spectra is assigned to the presence of the carboxylate ion COO.[62,63] The XPS data is consistent with FTIR and the formation of a titanium carboxylate film for all processes.

Stability. The majority of the peaks in the FTIR spectra is observed to remain identical over time up to 50 days of air exposure under ambient laboratory conditions. Only the broad O−H stretching vibration at 3600 cm^{-1} to 2500 cm^{-1} is found to increase. The observations indicate that the thin films are stable in air, but absorb water from ambient atmosphere. Other hybrid MLD films such as alucone and magnesicone also have shown the tendency to

Table 2: The atomic percentages (at. %) of all regions and components derived from the XPS spectra in figure 3. For the thinner films, Si from the Si-substrate is still visible.

	TDMAT/ oxalic acid	**TDMAT/ succinic acid**	**TDMAT/ glutaric acid**	**TDMAT/3,6-di-oxaoctanedioic acid**
Ti	13	11	10	11
O−Ti	20	17	15	15
OOC	23	18	18	17
N−C	6	4	4	5
COO	17	12	12	8
C−O/ C−N	15	10	9	18
C−C/ C−H	6	25	30	22
Si	-	3	2	4

absorb water from ambient atmosphere. But in contrast to the films deposited in the current work, these metalcone films are considered air-sensitive as the organic backbone degrades upon exposure. Due to the conformal and pinhole free deposition principle of ALD/MLD and the flexibility of hybrid MLD layers, MLD films show great potential for encapsulation applications.[42,69,70] The stability of the films when immersed into water is further investigated with FTIR and XRR and is shown in Figure S3 in the supporting information. Again it is observed that the O−H stretching vibration increases, indicating the absorption of water. At the same time the carboxylate stretching vibrations disappear and the film thickness decreases, implying the degradation of the film upon immersion in water. In literature, the degradation of hybrid MLD films upon exposure to water is typically assigned to hydrolysis of the chemical bonds.[71–73]

The stability of the films inside a liquid electrolyte solution of 1 M $LiClO_4$ in propylene carbonate used for electrochemical evaluation, is investigated with FTIR, XRR and X-ray Fluorescence (XRF) (data shown in Figure S4 in the supporting information). Minor changes are observed in the FTIR spectra which can all be ascribed to polyethylene carbonate molecules

from the solvent adhering to the surface. No change in thickness is observed after immersion into the electrolyte solution and the ratio of Ti/Si XRF counts before and after electrolyte immersion is comparable. The data thus suggests that the films are stable inside the electrolyte solution.

Comparison with literature. Only two reports mentioning the deposition of a hybrid metal carboxylate MLD film using saturated carboxylic acids, are found in literature. Klepper et al.[23] monitored the deposition of aluminium carboxylate films using TMA and various saturated dicarboxylic acids inside a ASM F-120 SAT reactor with in situ quartz crystal microbalance (QCM). Similar to this work, 'near' self-limiting growth kinetics were observed for the oxalic acid process at 186 °C, while more complex growth kinetics were observed for the malonic and glutaric acid process. In contrast to the current work, 'near' self-limiting growth kinetics were also observed for the succinic acid process and they did not observe the decomposition of malonic acid when heating the malonic acid up to 125 °C. This discrepancy can be ascribed to the short residence time of a precursor in the ASM F-120 SAT reactor compared to the usage time of a precursor bubbler used for deposition in the current work.

Compared to this work, Klepper et al.[23] found a smaller Δ of 129 cm^{-1} and 119 cm^{-1} for the TMA/succinic acid and TMA/glutaric acid films respectively, and thus also concluded a combination of chelating and bridging complexes present inside the succinic acid films, while the interaction in the glutaric acid films were mainly of the chelating type. The deposited aluminium carboxylate films were observed to be stable in air up to a year. It is reported that no measurable change could be observed with FTIR and XRR (data not shown) and thus no absorption of water from ambient air would take place. In addition, they claim their films are stable in contact with water, except for the oxalic and malonic acid based films, but apart from a water contact angle measurement no detailed study of the water stability upon immersion was performed.

Momtazi et al.[24] investigated the deposition of a titanium carboxylate films using TTIP and succinic acid. In contrast to the parasitic CVD component observed in this work, they observed 'near' self limiting growth kinetics with in situ QCM and obtained a maximum GPC of 0.14 nm/cycle at 180 °C. The resulting film was found to be of chelating type with a Δ of 90 cm^{-1}. They also investigated the effect of an extra water vapour pulse on the growth dynamics of the TTIP/succinic acid film. They found the film behaved similar to a sponge i.e. the film absorbed a large amount of water during the water pulse which again desorbed during the purge step. The overall growth-rate of the process was found to decrease by the addition of water, indicating the partial degradation of the organic linkers due to the exposure to water vapour.

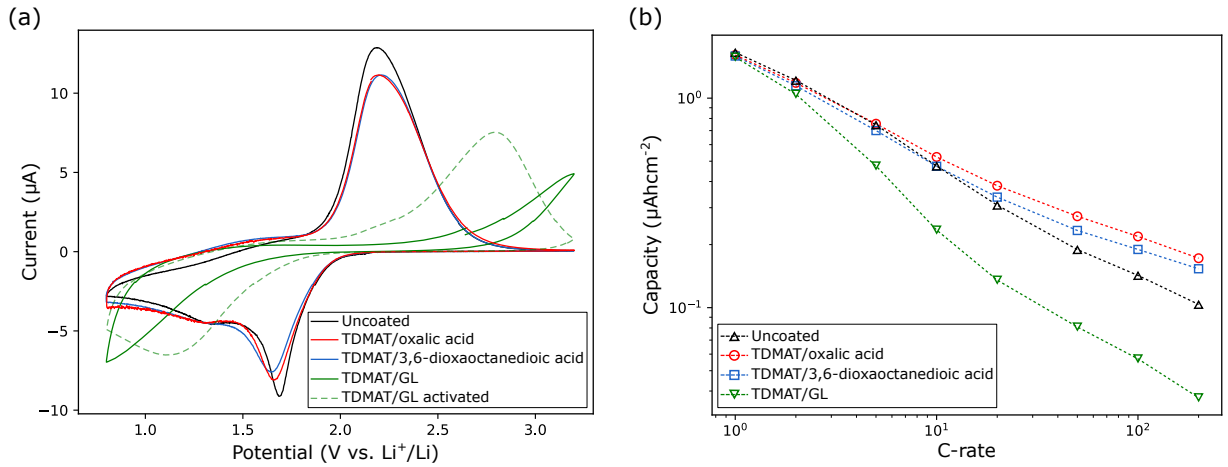

Figure 4: Cyclic voltammogram of the uncoated and 5 nm MLD coated 40 nm anatase TiO_2 electrodes.(a) The potential is varied between 0.8 V to 3.2 V vs Li^+/Li at 1 mV s^{-1}. The activated TDMAT/GL film displayed by a dashed line is used to to study the rate capability. The lithiation capacity densities of the (un)coated TiO_2 electrodes at various C-rates.(b) 1 C corresponds to charging and discharging with 2 μA h between 1.0 V to 3.0 V vs Li^+/Li.

Electrochemical characterization. The electrochemical properties of two titanium carboxylate films and a titanicone MLD film are evaluated. From all titanium carboxylate films that were discussed previously, the TDMAT/oxalic acid films that have the shortest organic backbone and the TDMAT/3,6-dioxaoctanedioic acid films that contain ethylene oxide units are selected. The films are compared to a titanicone film, a more conventional

type of 'metalcone' MLD film, deposited using TDMAT and GL.[35]

First, the ionic transparency of lithium-ions is analysed by depositing approximately 5 nm of the films on top of a 40 nm anatase TiO_2 reference electrode.[16] The cyclic voltammogram of the coated and uncoated electrode is shown in Figure 4 a. For both the titanium carboxylate films a small drop in peak current is observed compared to the uncoated electrode, which might indicate a small blocking effect of the coating. The TDMAT/GL film on the other hand shows a much more significant change in peak shape and position, indicating a detrimental effect on the electrode stack's kinetics. Upon prolonged cycling the voltammogram of the TDMAT/GL film improves, indicating that an 'activation' step is needed (data shown in supporting information Figure S5). But, even after activation, a large drop and shift in peak current remains visible as shown by the dashed line in Figure 4 a. The decrease in kinetics for the TDMAT/GL film is also observed when studying the rate capability of the (un)coated electrodes (Figure 4 b). For the two titanium carboxylate films only minor changes are observed compared to the uncoated electrode, meaning that the slight decrease observed in the cyclic voltammogram has little to no effect on the electrode's lithium ion kinetics. The films even seem to show a slight improvement at high C-rates, which might point towards minor electrochemical activity of the coating itself as was also observed by Mattelaer et al.[16] when applying an amorphous TiO_2 film to the TiO_2 electrode. As little to no effect is observed between the two different titanium carboxylate films on the lithium-ion kinetics of the underlying electrode, it is impossible to conclude that the incorporation of ethylene oxide units in the titanium carboxylate films increases the lithium-ion conductivity. To accurately determine the difference in lithium-ion conductivity, more research should be conducted using various thicknesses of the films and impedance spectroscopy.

The lithium-ions managed to be transmitted through the coatings, but it is also important to check whether the films have a protective function. For example, electrolyte oxidation will occur at the cathode at high potentials vs. Li^+/Li, causing the formation of a decomposition

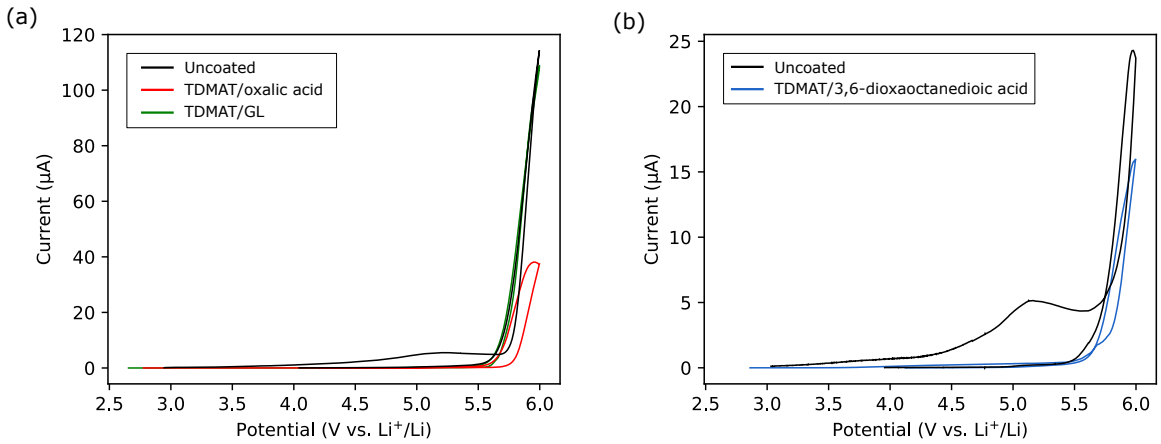

Figure 5: Cyclic voltammogram of the uncoated and 5 nm MLD coated TiN electrodes. The electrolyte decomposition on the TDMAT/oxalic acid and TDMAT/GL (a) and the TDMAT/3,6−dioxaoctanedioic acid coated electrode (b) is compared to an uncoated reference electrode which is measured simultaneously. The cells are cycled from open cell potential to 6 V vs Li^+/Li at a scan rate of 1 mV s^{-1}.

layer, leading to irreversible lithium loss and decreased (de)lithiation kinetics.[4,16,74,75] To analyse the protective function of the MLD films against electrolyte oxidation, a TiN electrode is coated with 5 nm of the MLD films and cycled up to 6 V. The electrolyte decomposition in these extreme conditions is highly dependent on the exact experimental parameters such as the electrolyte composition and temperature. To enable a direct comparison, the coated and uncoated reference electrode are always measured simultaneously. As TiN itself is not electrochemically active, the current that is observed in the cyclic voltammogram is either resulting from the coating on top, or from the irreversible electrolyte oxidation reaction. The results in Figure 5 displays the current at 5 V drops with 98.8 %, 92.6 % and 99.1 % for the 5 nm TDMAT/oxalic acid, TDMAT/3,6-dioxaoctanedioic acid and TDMAT/GL coated electrodes respectively compared to the uncoated reference. All coatings are thus able to suppress the electrolyte oxidation at elevated potential. As discussed earlier, in contrast to the TDMAT/GL films the two new titanium carboxylate films also maintain good lithium kinetics of the underlying electrode, making them promising protective coating materials for future cathodes. More research is needed to further optimize the films e.g. it is known from literature that both the lithium-ion kinetics and the protective properties are highly

depending on the thickness of the films.[16]

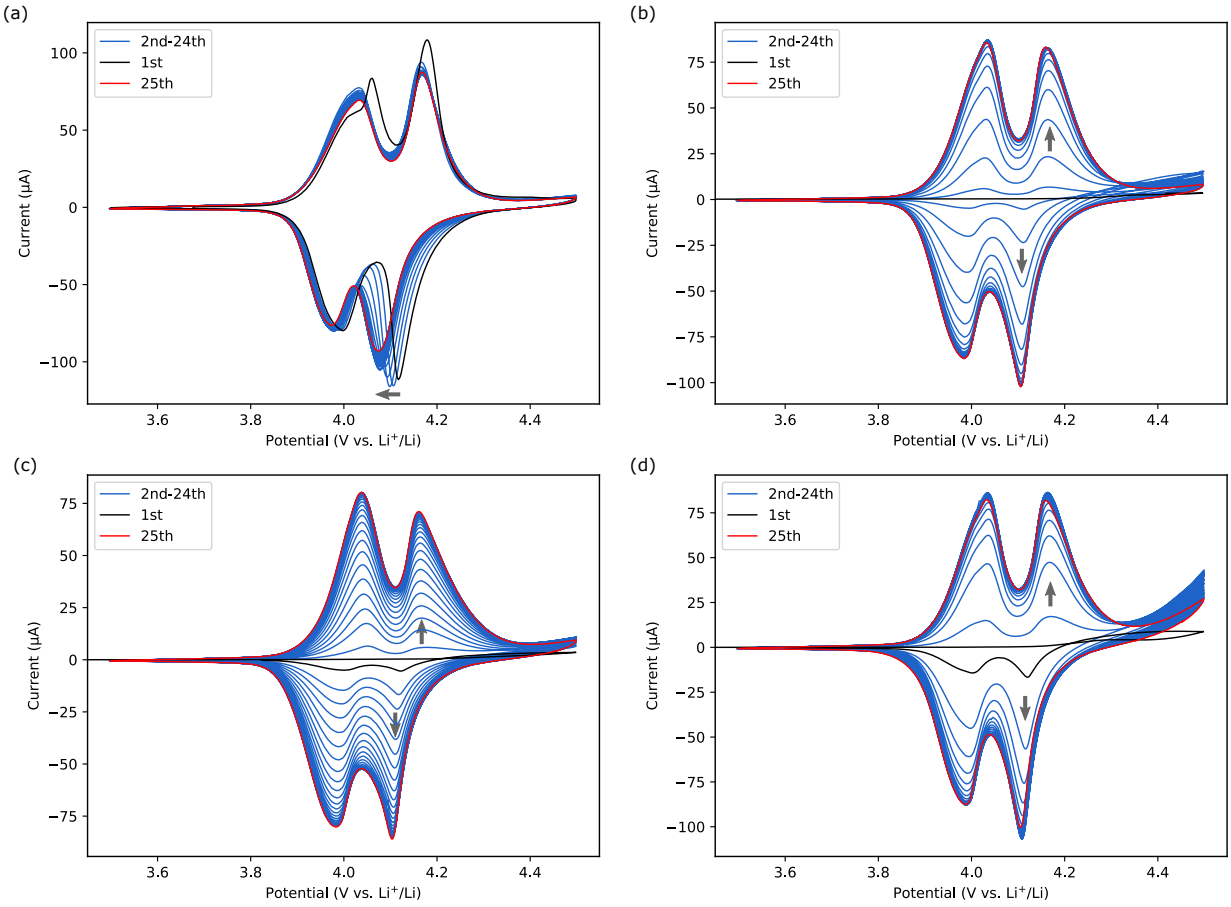

Figure 6: The first 25 cyclic voltammograms on the uncoated (a), TDMAT/oxalic acid (b), TDMAT/3,6−dioxaoctanedioic acid (c) and conventional TDMAT/GL (d) coated 100 nm PVD LMO electrodes. The cells are cycled between 3.5 V to 4.5 V vs Li^+/Li with a scan rate of 1 mV s^{-1}. The most important trends are indicated by grey arrows.

So far, the lithium kinetics was analysed on ideal electrode stacks. However, this doesn't necessarily mean the coatings will behave similarly on a realistic lithium-ion battery cathode operating at high potentials. Therefore, electrochemical characterization of the MLD films is performed on top of a 100 nm LMO electrode which is cycled between 3.5 V and 4.5 V vs. Li^+/Li. LMO is a commonly used lithium-ion battery cathode, suffering from Mn dissolution and volume changes caused by the Jahn-Teller distortion.[4,6,76] For example, for the uncoated electrode a clear shift of the anodic peak current around 4.1 V is visible during the first 25 cycles in the cyclic voltammogram as displayed in Figure 6. This shift might

be caused by the dissolution of Mn which is accelerated at higher potentials.[6] For the MLD coated electrodes the position of the peak currents are constant, but the peak currents are observed to increase upon cycling, indicating that an 'activation step' is needed for all MLD films on top of LMO. The increasing peak current translates into an increasing lithiation capacity and an increasing coulombic efficiency as can be seen in Figure S6 in supporting information. Both values seem to saturate at a constant value for the two titanium carboxylate films. The final coulombic efficiency after 25 cycles is 95 %, 92 %, 90 % and 76 % for the uncoated, TDMAT/oxalic acid, TDMAT/3,6-dioxaoctanedioic acid and TDMAT/GL coated LMO electrodes respectively. Comparison of the XRF counts before and after the electrochemical measurement, indicate the films are still present on the LMO surface (data shown in Table S2 in supporting information). Ideally, to further evaluate the stability of the films capacity retention tests should be performed.

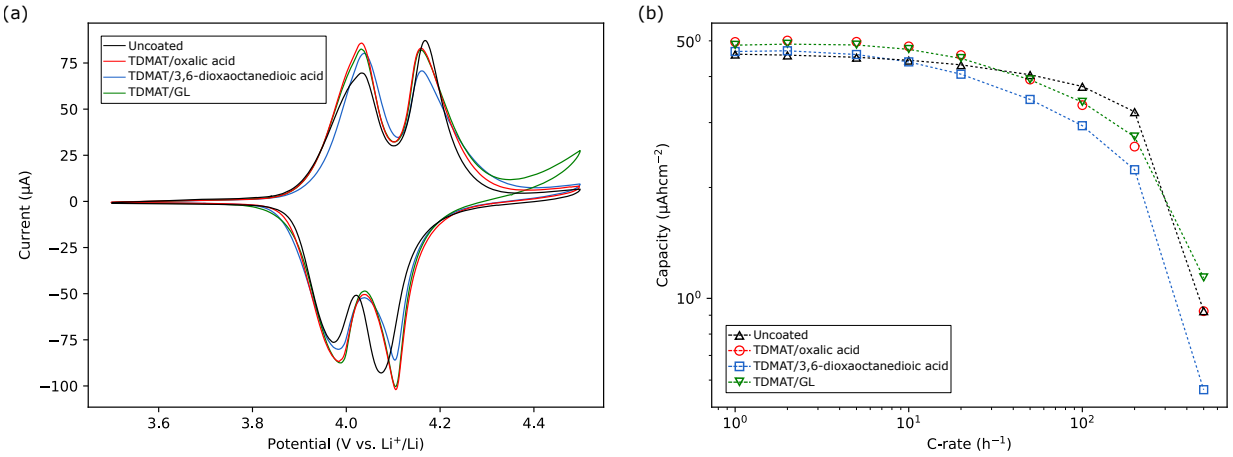

Figure 7: The 25th cyclic voltammogram of the uncoated and 5 nm MLD coated 100 nm LMO electrodes.(a) The cells are cycled between 3.5 V to 4.5 V at a scan rate of 1 mV s^{-1}. The lithiation capacity densities of the (un)coated LMO electrodes at various C-rates.(b) 1 C corresponds to charging and discharging with 6 µA h between 3.5 V to 4.5 V vs Li^+/Li.

The 25th cyclic voltammogram of the MLD films on LMO in Figure 7 a displays only minor differences in peak current and position compared to the uncoated reference electrode. In addition, only a small effect of the coatings on top of the LMO electrode can be seen in the lithiation capacity at different C-rates in Figure 7 b. For the TDMAT/GL film some

irreversible reactions are observed during the first lithiation and delithiation step, which can be seen clearly in the potential profile and is shown in Figure S7 in supporting information. Overall, the two titanium carboxylate films present a good lithium-ion mobility through the coating without the irreversible reactions that are observed for the TDMAT/GL MLD film on LMO. It can be hypothesized that the titanium carboxylate films are electrochemically more stable due to the incorporation of carboxylates into the MLD films, forming a chemical environment resembling the carbonates that are present in the liquid electrolyte. This hypothesis should be investigated into more depth using different liquid electrolytes and various organic linkers and might ultimately lead to selection principles for the organic precursor.

4 Conclusion

Titanium carboxylate films are successfully deposited using TDMAT and various dicarboxylic acid precursors. Only the TDMAT/oxalic acid process displays good MLD saturation behaviour at 100 °C and 160 °C. For the other processes a parasitic CVD component is present during the TDMAT pulse. All as-deposited films are observed to be stable in air. The films are found to absorb water from ambient atmosphere, while the organic backbone remains intact, in contrast to most metalcone MLD films. The titanium carboxylate films are found to remain intact when immersed into a solution of 1 M $LiClO_4$ in propylene carbonate used as electrolyte during electrochemical characterization. Overall the electrochemical properties of the titanium carboxylate films seem promising as protective coatings for cathode materials in lithium-ion batteries. An activation step is needed on LMO, but the films display a good lithium ion mobility, can effectively suppress electrolyte decomposition at high voltages and present less irreversible electrochemical reactions compared to a titanicone MLD film deposited using TDMAT and GL. More research is needed to further optimize and test these coatings on commercial powder-based battery cathodes. However,

the exploratory tests on thin film electrodes seem promising for the future use of MLD films as protective and flexible coatings for lithium-ion battery cathodes.

Supporting Information

Saturation data of the TDMAT/dicarboxylic acid processes at 160 °C; Comparison of the refractive index and density of the films deposited at 100 °C and 160 °C; XPS spectra of TDMAT/oxalic acid MLD films deposited at 100 °C and 160 °C; Stability of the titanium carboxylate films in water measured by FTIR and XRR; Stability of the titanium carboxylate films in an electrolyte solution of 1 M $LiClO_4$ in propylene carbonate measured by FTIR, XRR and XRF; Electrochemical activation of titanicone on the 40 nm anatase TiO_2 electrode; Evolution of the coulombic efficiency and lithiation capactity of the (un)coated LMO electrodes; Stability of the films on the LMO electrode upon cycling measured by XRF; Potential profiles of the first and second lithiation and delithiation of the (un)coated LMO electrodes.

Acknowledgements

The authors acknowledge BOF-UGent (GOA-01G01019) for financial support.

References

(1) Li, M.; Lu, J.; Chen, Z.; Amine, K. 30 Years of Lithium-Ion Batteries. *Advanced Materials* **2018**, *30*, 1800561.

(2) Crabtree, G.; Kocs, E.; Trahey, L. The Energy-Storage Frontier: Lithium-Ion Batteries and Beyond. *Mrs Bulletin* **2015**, *40*, 1067–1078.

(3) Yoshino, A. The Birth of the Lithium-Ion Battery. *Angewandte Chemie International Edition* **2012**, *51*, 5798–5800.

(4) Vetter, J.; Novák, P.; Wagner, M. R.; Veit, C.; Möller, K.-C.; Besenhard, J.; Winter, M.; Wohlfahrt-Mehrens, M.; Vogler, C.; Hammouche, A. Ageing Mechanisms in Lithium-Ion Batteries. *Journal of power sources* **2005**, *147*, 269–281.

(5) Li, W.; Song, B.; Manthiram, A. High-Voltage Positive Electrode Materials for Lithium-Ion Batteries. *Chemical Society Reviews* **2017**, *46*, 3006–3059.

(6) Zhan, C.; Wu, T.; Lu, J.; Amine, K. Dissolution, Migration, and Deposition of Transition Metal Ions in Li-Ion Batteries Exemplified by Mn-Based Cathodes–A Critical Review. *Energy & Environmental Science* **2018**, *11*, 243–257.

(7) Fu, L.; Liu, H.; Li, C.; Wu, Y.; Rahm, E.; Holze, R.; Wu, H. Surface Modifications of Electrode Materials for Lithium Ion Batteries. *Solid State Sciences* **2006**, *8*, 113–128.

(8) Li, C.; Zhang, H.; Fu, L.; Liu, H.; Wu, Y.; Rahm, E.; Holze, R.; Wu, H. Cathode Materials Modified by Surface Coating for Lithium Ion Batteries. *Electrochimica Acta* **2006**, *51*, 3872–3883.

(9) Chen, Z.; Qin, Y.; Amine, K.; Sun, Y.-K. Role Of Surface Coating on Cathode Materials for Lithium-Ion Batteries. *Journal of Materials Chemistry* **2010**, *20*, 7606–7612.

(10) George, S. M. Atomic Layer Deposition: An Overview. *Chemical reviews* **2010**, *110*, 111–131.

(11) Puurunen, R. L. Surface Chemistry of Atomic Layer Deposition: A Case Study for the Trimethylaluminum/Water Process. *Journal of applied physics* **2005**, *97*, 9.

(12) Cremers, V.; Puurunen, R. L.; Dendooven, J. Conformality in Atomic Layer Deposition: Current Status Overview of Analysis and Modelling. *Applied Physics Reviews* **2019**, *6*, 021302.

(13) Wise, A. M.; Ban, C.; Weker, J. N.; Misra, S.; Cavanagh, A. S.; Wu, Z.; Li, Z.; Whittingham, M. S.; Xu, K.; George, S. M.; Toney, M. F. Effect of Al_2O_3 Coating on Stabilizing $LiNi_{0.4}Mn_{0.4}Co_{0.2}O_2$ Cathodes. *Chemistry of Materials* **2015**, *27*, 6146–6154.

(14) Luan, X.; Guan, D.; Wang, Y. Enhancing High-Rate and Elevated-Temperature Performances of Nano-Sized and Micron-Sized $LiMn_2O_4$ in Lithium-Ion Batteries with Ultrathin Surface Coatings. *Journal of nanoscience and nanotechnology* **2012**, *12*, 7113–7120.

(15) Jung, Y. S.; Cavanagh, A. S.; Riley, L. A.; Kang, S.-H.; Dillon, A. C.; Groner, M. D.; George, S. M.; Lee, S.-H. Ultrathin Direct Atomic Layer Deposition on Composite Electrodes for Highly Durable and Safe Li-Ion Batteries. *Advanced Materials* **2010**, *22*, 2172–2176.

(16) Mattelaer, F.; Vereecken, P. M.; Dendooven, J.; Detavernier, C. The Influence of Ultrathin Amorphous ALD Alumina and Titania on the Rate Capability of Anatase TiO_2 and $LiMn_2O_4$ Lithium Ion Battery Electrodes. *Advanced Materials Interfaces* **2017**, *4*, 1601237.

(17) Ban, C.; George, S. M. Molecular Layer Deposition for Surface Modification of Lithium-Ion Battery Electrodes. *Advanced Materials Interfaces* **2016**, *3*, 1600762.

(18) Nilsen, O.; Klepper, K.; Nielsen, H.; Fjellvaåg, H. Deposition of Organic-Inorganic Hybrid Materials by Atomic Layer Deposition. *Ecs Transactions* **2008**, *16*, 3.

(19) George, S. M.; Yoon, B.; Dameron, A. A. Surface Chemistry for Molecular Layer Deposition of Organic and Hybrid Organic- Inorganic Polymers. *Accounts of Chemical Research* **2009**, *42*, 498–508.

(20) Sundberg, P.; Karppinen, M. Organic and Inorganic–Organic Thin Film Structures by Molecular Layer Deposition: A Review. *Beilstein journal of nanotechnology* **2014**, *5*, 1104–1136.

(21) Van Bui, H.; Grillo, F.; Van Ommen, J. Atomic and Molecular Layer Deposition: Off the Beaten Track. *Chemical Communications* **2017**, *53*, 45–71.

(22) George, S. M.; Lee, B. H.; Yoon, B.; Abdulagatov, A. I.; Hall, R. A. Metalcones: Hybrid Organic–Inorganic Films Fabricated Using Atomic and Molecular Layer Deposition Techniques. *Journal of nanoscience and nanotechnology* **2011**, *11*, 7948–7955.

(23) Klepper, K. B.; Nilsen, O.; Hansen, P.-A.; Fjellvåg, H. Atomic Layer Deposition of Organic–Inorganic Hybrid Materials Based on Saturated Linear Carboxylic Acids. *Dalton Transactions* **2011**, *40*, 4636–4646.

(24) Momtazi, L.; Sønsteby, H. H.; Dartt, D.; Eidet, J. R.; Nilsen, O. Bioactive Titaminates from Molecular Layer Deposition. *RSC advances* **2017**, *7*, 20900–20907.

(25) Zhao, Y.; Sun, X. Molecular Layer Deposition for Energy Conversion and Storage. *ACS Energy Letters* **2018**, *3*, 899–914.

(26) Zhao, Y.; Zhang, L.; Liu, J.; Adair, K.; Zhao, F.; Sun, Y.; Wu, T.; Bi, X.; Amine, K.; Lu, J.; Sun, X. Atomic/Molecular Layer Deposition for Energy Storage and Conversion. *Chemical Society Reviews* **2021**, *50*, 3889–3956.

(27) Piper, D. M.; Travis, J. J.; Young, M.; Son, S.-B.; Kim, S. C.; Oh, K. H.; George, S. M.; Ban, C.; Lee, S.-H. Reversible High-Capacity Si Nanocomposite Anodes for Lithium-Ion Batteries Enabled by Molecular Layer Deposition. *Advanced Materials* **2014**, *26*, 1596–1601.

(28) Piper, D. M.; Lee, Y.; Son, S.-B.; Evans, T.; Lin, F.; Nordlund, D.; Xiao, X.; George, S. M.; Lee, S.-H.; Ban, C. Cross-Linked Aluminum Dioxybenzene Coating for Stabilization of Silicon Electrodes. *Nano Energy* **2016**, *22*, 202–210.

(29) He, Y.; Piper, D. M.; Gu, M.; Travis, J. J.; George, S. M.; Lee, S.-H.; Genc, A.; Pullan, L.; Liu, J.; Mao, S. X.; Zhang, J.-G.; Ban, C.; Wang, C. In Situ Transmission

Electron Microscopy Probing of Native Oxide and Artificial Layers on Silicon Nanoparticles for Lithium Ion Batteries. *ACS nano* **2014**, *8*, 11816–11823.

(30) Li, X.; Lushington, A.; Liu, J.; Li, R.; Sun, X. Superior Stable Sulfur Cathodes of Li–S Batteries Enabled by Molecular Layer Deposition. *Chemical Communications* **2014**, *50*, 9757–9760.

(31) Li, X.; Lushington, A.; Sun, Q.; Xiao, W.; Liu, J.; Wang, B.; Ye, Y.; Nie, K.; Hu, Y.; Xiao, Q.; Li, R.; Guo, J.; Sham, T.-K.; Sun, X. Safe and Durable High-Temperature Lithium–Sulfur Batteries via Molecular Layer Deposited Coating. *Nano letters* **2016**, *16*, 3545–3549.

(32) Zhao, Y.; Goncharova, L. V.; Sun, Q.; Li, X.; Lushington, A.; Wang, B.; Li, R.; Dai, F.; Cai, M.; Sun, X. Robust Metallic Lithium Anode Protection by The Molecular-Layer-Deposition Technique. *Small Methods* **2018**, *2*, 1700417.

(33) Mu, T.; Zhao, Y.; Zhao, C.; Holmes, N. G.; Lou, S.; Li, J.; Li, W.; He, M.; Sun, Y.; Du, C.; Li, R.; Wang, J.; Yin, G.; Sun, X. Stable Silicon Anodes by Molecular Layer Deposited Artificial Zincone Coatings. *Advanced Functional Materials* **2021**, *31*, 2010526.

(34) Xue, Z.; He, D.; Xie, X. Poly(ethylene oxide)-Based Electrolytes for Lithium-Ion Batteries. *Journal of Materials Chemistry A* **2015**, *3*, 19218–19253.

(35) Van de Kerckhove, K.; Mattelaer, F.; Deduytsche, D.; Vereecken, P. M.; Dendooven, J.; Detavernier, C. Molecular Layer Deposition of "Titanicone", a Titanium-Based Hybrid Material, as an Electrode for Lithium-Ion Batteries. *Dalton Transactions* **2016**, *45*, 1176–1184.

(36) Biesinger, M. C.; Lau, L. W.; Gerson, A. R.; Smart, R. S. C. Resolving Surface Chemical States in XPS Analysis of First Row Transition Metals, Oxides and Hydroxides: Sc, Ti, V, Cu and Zn. *Applied surface science* **2010**, *257*, 887–898.

(37) Dobbelaere, T.; Vereecken, P. M.; Detavernier, C. A USB-Controlled Potentiostat/Galvanostat for Thin-Film Battery Characterization. *HardwareX* **2017**, *2*, 34–49.

(38) Put, B.; Vereecken, P. M.; Labyedh, N.; Sepulveda, A.; Huyghebaert, C.; Radu, I. P.; Stesmans, A. High Cycling Stability and Extreme Rate Performance in Nanoscaled $LiMn_2O_4$ Thin Films. *ACS applied materials & interfaces* **2015**, *7*, 22413–22420.

(39) Bernoulli, A.; Wege, W. Reaktionskinetische Studien an substituierten Malonsäuren. *Helvetica Chimica Acta* **1919**, *2*, 511–532.

(40) Hinshelwood, C. N. XX.—The Rate of Decomposition of Malonic Acid. *Journal of the Chemical Society, Transactions* **1920**, *117*, 156–165.

(41) Brown, B. The Mechanism of Thermal Decarboxylation. *Quarterly Reviews, Chemical Society* **1951**, *5*, 131–146.

(42) Kint, J.; Mattelaer, F.; Vandenbroucke, S. S.; Muriqi, A.; Minjauw, M. M.; Nisula, M.; Vereecken, P. M.; Nolan, M.; Dendooven, J.; Detavernier, C. Molecular Layer Deposition of "Magnesicone", a Magnesium-based Hybrid Material. *Chemistry of Materials* **2020**, *32*, 4451–4466.

(43) Klepper, K. B.; Nilsen, O.; Fjellvåg, H. Deposition of Thin Films of Organic–Inorganic Hybrid Materials Based on Aromatic Carboxylic Acids by Atomic Layer Deposition. *Dalton Transactions* **2010**, *39*, 11628–11635.

(44) Yoon, B.; O'Patchen, J. L.; Seghete, D.; Cavanagh, A. S.; George, S. M. Molecular Layer Deposition of Hybrid Organic-Inorganic Polymer Films using Diethylzinc and Ethylene Glycol. *Chemical Vapor Deposition* **2009**, *15*, 112–121.

(45) Jain, H.; Poodt, P. About the Importance of Purge Time in Molecular Layer Deposition of Alucone Films. *Dalton Transactions* **2021**, *50*, 5807–5818.

(46) Socrates, G. *Infrared and Raman Characteristic Group Frequencies: Tables and Charts*, 3rd ed.; John Wiley & Sons: Chichester, 2001; pp 50–53, 94–95, 101–102, 125–139, 271.

(47) Silverstien, R.; Webster, I.; Kiemle, D. *Spectrometric Identification of Organic Compounds*, 7th ed.; John Wiley & Sons Inc.: New York, 2005; pp 95–97.

(48) Lin-Vien, D.; Colthup, N. B.; Fateley, W. G.; Grasselli, J. G. *The Handbook of Infrared and Raman Characteristic Frequencies of Organic Molecules*; Academic Press: San Diego, 1991; pp 9–14, 137–141.

(49) Tao, W.; Fei, F.; Yue-Chuan, W. Structure and Thermal Properties of Titanium Dioxide-Polyacrylate Nanocomposites. *Polymer Bulletin* **2006**, *56*, 413–426.

(50) Gao, X.; Zhang, Y.; Liu, Y. Temperature-Dependent Hygroscopic Behaviors of Atmospherically Relevant Water-Soluble Carboxylic Acid Salts Studied by ATR-FTIR Spectroscopy. *Atmospheric Environment* **2018**, *191*, 312–319.

(51) Perrin, F.; Nguyen, V.; Vernet, J. FT-IR Spectroscopy of Acid-Modified Titanium Alkoxides: Investigations on the Nature of Carboxylate Coordination and Degree of Complexation. *Journal of sol-gel science and technology* **2003**, *28*, 205–215.

(52) Hug, S. J.; Bahnemann, D. Infrared Spectra of Oxalate, Malonate and Succinate Adsorbed on the Aqueous Surface of Rutile, Anatase and Lepidocrocite Measured with In Situ ATR-FTIR. *Journal of electron spectroscopy and related phenomena* **2006**, *150*, 208–219.

(53) Fujita, J.; Nakamoto, K.; Kobayashi, M. Infrared Spectra of Metallic Complexes. III. The Infrared Spectra of Metallic Oxalates. *The Journal of Physical Chemistry* **1957**, *61*, 1014–1015.

(54) Martin, D.; Cole, R.; Haq, S. Investigating the Adsorption of Oxalic Acid Onto Cu (110) to Create a Chemically Functionalised Surface. *Surface science* **2003**, *539*, 171–181.

(55) Ito, K.; Bernstein, H. J. The Vibrational Spectra of the Formate, Acetate, and Oxalate Ions. *Canadian Journal of Chemistry* **1956**, *34*, 170–178.

(56) Verpoort, F.; Haemers, T.; Roose, P.; Maes, J.-P. Characterization of a Surface Coating Formed from Carboxylic Acid-Based Coolants. *Applied Spectroscopy* **1999**, *53*, 1528–1534.

(57) Deacon, G.; Phillips, R. Relationships Between the Carbon-Oxygen Stretching Frequencies of Carboxylato Complexes and the Type of Carboxylate Coordination. *Coordination Chemistry Reviews* **1980**, *33*, 227–250.

(58) Doeuff, S.; Henry, M.; Sanchez, C.; Livage, J. Hydrolysis of Titanium Alkoxides: Modification of the Molecular Precursor by Acetic Acid. *Journal of Non-crystalline solids* **1987**, *89*, 206–216.

(59) Pucić, I.; Jurkin, T. FTIR Assessment of Poly(ethylene oxide) Irradiated in Solid State, Melt and Aqeuous Solution. *Radiation Physics and Chemistry* **2012**, *81*, 1426–1429.

(60) Zhang, F.; Jin, S.; Mao, Y.; Zheng, Z.; Chen, Y.; Liu, X. Surface Characterization of Titanium Oxide Films Synthesized by Ion Beam Enhanced Deposition. *Thin Solid Films* **1997**, *310*, 29–33.

(61) Mayer, J.; Diebold, U.; Madey, T.; Garfunkel, E. Titanium and Reduced Titania Overlayers on Titanium Dioxide (110). *Journal of Electron Spectroscopy and Related Phenomena* **1995**, *73*, 1–11.

(62) Cano, E.; Torres, C.; Bastidas, J. An XPS Study of Copper Corrosion Originated by Formic Acid Capour at 40% and 80% Relative Humidity. *Materials and Corrosion* **2001**, *52*, 667–676.

(63) Rajagopalan, R.; Iroh, J. O. Characterization of Polyaniline–Polypyrrole Composite

Coatings on Low Carbon Steel: A XPS and Infrared Spectroscopy Study. *Applied Surface Science* **2003**, *218*, 58–69.

(64) Schnadt, J.; O'shea, J.; Patthey, L.; Schiessling, J.; Krempaskỳ, y. J.; Shi, M.; Mårtensson, N.; Brühwiler, P. Structural Study of Adsorption of Isonicotinic Acid and Related Molecules on Rutile TiO_2 (1 1 0) II: XPS. *Surface science* **2003**, *544*, 74–86.

(65) Singh, J.; Gusain, A.; Saxena, V.; Chauhan, A.; Veerender, P.; Koiry, S.; Jha, P.; Jain, A.; Aswal, D.; Gupta, S. XPS, UV–Vis, FTIR, and EXAFS Studies to Investigate The Binding Mechanism of N719 Dye Onto Oxalic Acid Treated TiO_2 and Its Implication on Photovoltaic Properties. *The Journal of Physical Chemistry C* **2013**, *117*, 21096–21104.

(66) Vandenbroucke, S. S.; Levrau, E.; Minjauw, M. M.; Van Daele, M.; Solano, E.; Vos, R.; Dendooven, J.; Detavernier, C. Study of the Surface Species During Thermal and Plasma-Enhanced Atomic Layer Deposition of Titanium Oxide Films Using In Situ IR-Spectroscopy and In Vacuo X-Ray Photoelectron Spectroscopy. *Physical Chemistry Chemical Physics* **2020**, *22*, 9262–9271.

(67) Head, A. R.; Chaudhary, S.; Olivieri, G.; Bournel, F.; Andersen, J. N.; Rochet, F.; Gallet, J.-J.; Schnadt, J. Near Ambient Pressure X-Ray Photoelectron Spectroscopy Study of the Atomic Layer Deposition of TiO_2 on RuO_2 (110). *The Journal of Physical Chemistry C* **2016**, *120*, 243–251.

(68) Graf, N.; Yegen, E.; Gross, T.; Lippitz, A.; Weigel, W.; Krakert, S.; Terfort, A.; Unger, W. E. XPS and NEXAFS Studies of Aliphatic and Aromatic Amine Species on Functionalized Surfaces. *Surface Science* **2009**, *603*, 2849–2860.

(69) Peñaranda, J. S. D.; Nisula, M.; Vandenbroucke, S. S.; Minjauw, M. M.; Li, J.; Werbrouck, A.; Keukelier, J.; Martínez, A. I. P.; Dendooven, J.; Detavernier, C. Converting

Molecular Layer Deposited Alucone Films into Al_2O_3/Alucone Hybrid Multilayers by Plasma Densification. *Dalton Transactions* **2021**, *50*, 1224–1232.

(70) Jen, S.-H.; Lee, B. H.; George, S. M.; McLean, R. S.; Carcia, P. F. Critical Tensile Strain and Water Vapor Transmission Rate for Nanolaminate Films Grown Using Al_2O_3 Atomic Layer Deposition and Alucone Molecular Layer Deposition. *Applied Physics Letters* **2012**, *101*, 234103.

(71) Yang, F.; Brede, J.; Ablat, H.; Abadia, M.; Zhang, L.; Rogero, C.; Elliott, S. D.; Knez, M. Reversible and Irreversible Reactions of Trimethylaluminum with Common Organic Functional Groups as a Model for Molecular Layer Deposition and Vapor Phase Infiltration. *Advanced Materials Interfaces* **2017**, *4*, 1700237.

(72) Choi, D.-w.; Yoo, M.; Lee, H. M.; Park, J.; Kim, H. Y.; Park, J.-S. A Study on the Growth Behavior and Stability of Molecular Layer Deposited Alucone Films Using Diethylene Glycol and Trimethyl Aluminum Precursors, and the Enhancement of Diffusion Barrier Properties by Atomic Layer Deposited Al_2O_3 Capping. *ACS Applied Materials & Interfaces* **2016**, *8*, 12263–12271.

(73) Bergsman, D. S.; Baker, J. G.; Closser, R. G.; MacIsaac, C.; Lillethorup, M.; Strickler, A. L.; Azarnouche, L.; Godet, L.; Bent, S. F. Structurally Stable Manganese Alkoxide Films Grown by Hybrid Molecular Layer Deposition for Electrochemical Applications. *Advanced Functional Materials* **2019**, *29*, 1904129.

(74) Wang, A.; Kadam, S.; Li, H.; Shi, S.; Qi, Y. Review on Modeling of the Anode Solid Electrolyte Interphase (SEI) for Lithium-Ion Batteries. *npj Computational Materials* **2018**, *4*, 1–26.

(75) Verma, P.; Maire, P.; Novák, P. A Review of the Features and Analyses of the Solid Electrolyte Interphase in Li-Ion Batteries. *Electrochimica Acta* **2010**, *55*, 6332–6341.

(76) Goodenough, J. B.; Park, K.-S. The Li-Ion Rechargeable Battery: A Perspective. *Journal of the American Chemical Society* **2013**, *135*, 1167–1176.

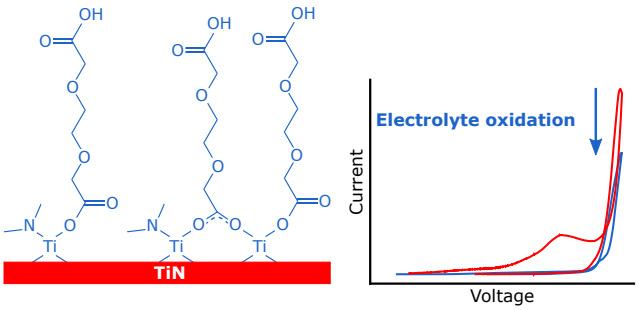

For Table of Contents Only.